FULL PAPER

Swelling-Induced Surface Patterns in Hydrogels with Gradient Crosslinking Density

By *Murat Guvendiren, Shu Yang,** and *Jason A. Burdick**

Hydrogels with controlled surface patterns are useful for a range of applications, including in microdevices, sensors, coatings, and adhesives. In this work, a simple and robust method to generate a wide range of osmotically driven surface patterns, including random, lamellar, peanut, and hexagonal structures is developed. This method does not require the use of organic solvents for swelling, pre-patterning of the film surface, or coating of a second layer on the gel. The patterns are fabricated by exposing a photocurable formulation to light while open to air and then swelling, using oxygen inhibition of the radical polymerization at the surface to create a gradient of crosslinking with depth, which was confirmed by measuring the double bond conversion at the surface, surface mechanics, and molecule diffusion into the network. The modulus gradient, and hence osmotic pressure, is controlled by the crosslinker concentration, and the characteristic size of the patterns is determined by the initial film thickness. The patterns are stable in both swollen and dry states, creating a versatile approach that is useful for diverse polymers to create complex patterns with long-range order.

1. Introduction

There is a growing interest in polymeric systems that display spontaneous formation of patterns with controlled size, order, morphology, and complexity, as they are useful for a wide range of applications, including sensors,[1,2] microfluidic devices,[3] responsive coatings,[4] smart adhesives,[5] microlens arrays,[6–8] and for controlling cellular behavior.[9] Buckling or wrinkling of a thin film on a compliant substrate is the most common method to obtain self-organized patterns with a wide range of morphology and complexity. The majority of studies performed in this field, originating from the pioneering work of Bowden et al.,[10] involve coating a thin hard skin, for example, metal,[11] polymers,[1,12] or silicate,[7,8,13] on a softer elastomer sheet, such as poly(dimethyl siloxane) (PDMS), which can be expanded thermally, mechanically, or osmotically. The modulus mismatch between the bilayers creates a compressive stress that triggers buckling, leading to the formation of various wrinkle patterns, including one-dimensional (1D) ripples, two-dimensional (2D) labyrinth and herringbone structures, and their variations.[14,15] The morphology, order, and complexity of the wrinkle patterns can be controlled by varying the uniformity of the physical properties and the dimensions of the materials.[10] However, the majority of these studies have focused on pattern formation above the critical stress, and few have demonstrated highly ordered hexagonal patterns with this wrinkling mechanism.[7,16] The length scales in these systems are typically on the order of submicrometer to tens of micrometers, due to the competition between the hard skin favoring the short wavelength wrinkles and the soft elastomer favoring the longer wavelength wrinkles.

Another system of interest to create various surface patterns via harnessing materials instability is hydrogels. In comparison to PDMS elastomers, there are a wide range of hydrogels with tunable chemistry and functionality that will allow us to manipulate their crosslinking density and gradient, and responsiveness to environmental stimuli (e.g., heat, light, electrical potential, chemicals, and biological agents), therefore offering much richer materials properties to create surface patterns than PDMS. Almost two decades ago, Tanaka et al.[17] reported on the evolution of swelling-induced surface patterns in acrylamide hydrogels constrained on a flat substrate. The pattern formation was attributed to the competition between osmotic pressure and mechanical constraints, or lateral confinement within the gel. Although the initial gel was crosslinked homogeneously, because it was fixed on a rigid flat substrate, only the top layer was free to expand, which generated an anisotropic osmotic pressure along the film thickness. This pressure increased with time as the gel was swollen. When the osmotic pressure was large enough, the outer surface was forced to buckle, resulting in the formation of surface patterns. The pattern formation was transient in nature depending on the osmotic pressure. Since this observation, many have attempted to manipulate the surface pattern formation in various hydrogels both experimentally[18–20] and theoretically.[21] However, the nonlinear nature of the gel swelling and lack of the control over osmotic pressure, which is always much greater than the critical value for buckling, make it challenging to control the long-range order and morphology of the final patterns.

[*] Prof. J. A. Burdick, Dr. M. Guvendiren
Department of Bioengineering
University of Pennsylvania
210 S 33th Street, Philadelphia, PA 19104 (USA)
E-mail: burdick2@seas.upenn.edu
Prof. S. Yang
Department of Materials Science and Engineering
University of Pennsylvania
3231 Walnut Street, Philadelphia, PA 19104 (USA)
E-mail: shuyang@seas.upenn.edu

DOI: 10.1002/adfm.200900622

Here, by combining the solvent-induced gel swelling and buckling effect due to modulus mismatch in a bilayer film, we report the dynamic evolution of a wide range of surface patterns in poly(hydroxyethyl methacrylate) (PHEMA) hydrogel films confined on a flat substrate, from a highly ordered hexagonal pattern in transit to peanut shape, lamellar, and random worm-like structures. The key difference from the prior reports on swelling-induced surface pattern formation is that we create a modulus gradient along the hydrogel film thickness by manipulating the UV curing process, thus allowing us to fine-tune the local osmotic pressure within the film toward the formation of a highly ordered hexagonal pattern. The resulting surface patterns are stable in both wet and dry states. Further study suggests that the equilibrium morphology is determined by the mechanical properties of the film (e.g., crosslinker concentration), whereas the characteristic wavelength of the pattern is controlled by the initial film thickness. Here we present a first step in understanding the importance of gel uniformity toward the ordering of surface patterns. We believe our study will shed light on forming complex patterns with long range ordering by harnessing instabilities in anisotropic soft gels.

2. Results and Discussion

PHEMA films were fabricated from a UV-curable precursor solution composed of partially polymerized PHEMA, a photoinitiator (Darocur 1173), and a crosslinker (ethylene glycol dimethacrylate, EGDMA). The precursor solution was spin-coated on to a substrate (silicon wafer or methacrylated glass slide) and exposed to UV light either open to air or covered to form a crosslinked film (Fig. 1). Initially, the precursor solution was well aerated and contained dissolved oxygen (typically $\sim 10^{-3}$ M[22]). It is well known that dissolved oxygen can consume radicals[22,23] and hence inhibit photopolymerization and crosslinking of polymers (Fig. S1a, Supporting Information) until dissolved oxygen is consumed to a minimal level. In an open air environment, oxygen continually diffused into the film from the air–film interface:[22,23]

$$\frac{d[O_2]}{dt} = D_O \frac{d[O_2]}{dz} - k_O[R][O_2] \quad (1)$$

where D_O is the oxygen diffusion constant ($\sim 10^{-6}$ cm^2 s^{-1}), k_o is the rate of oxidation ($\sim 5 \times 10^8$ L mol^{-1} s^{-1}), and $[R]$ and $[O_2]$ denote molar concentration of initiator and oxygen, respectively. It was evident from our experiments that, when the film thickness was less than 20 μm, more than 2 wt% crosslinker was necessary to form a crosslinked film by photocuring, indicating that when EGDMA < 2 wt%, $D_O d[O_2]/dz >> k_O[R][O_2]$. For films thicker than 20 μm, the consumed oxygen could not be replaced fast enough to limit crosslinking, and the amount of diffused oxygen gradually decreased along the film depth. With this in mind, it is possible to create a modulus gradient with depth such that the top surface (near air) has a lower crosslinking density and modulus, which gradually increases with film depth, and levels off after reaching the critical depth for oxygen diffusion (Fig. 2 and Fig. S1, Supporting Information). The profile of the crosslinking density gradient with depth can be modulated by the initiator and EGDMA concentrations, precursor viscosity, exposure time and

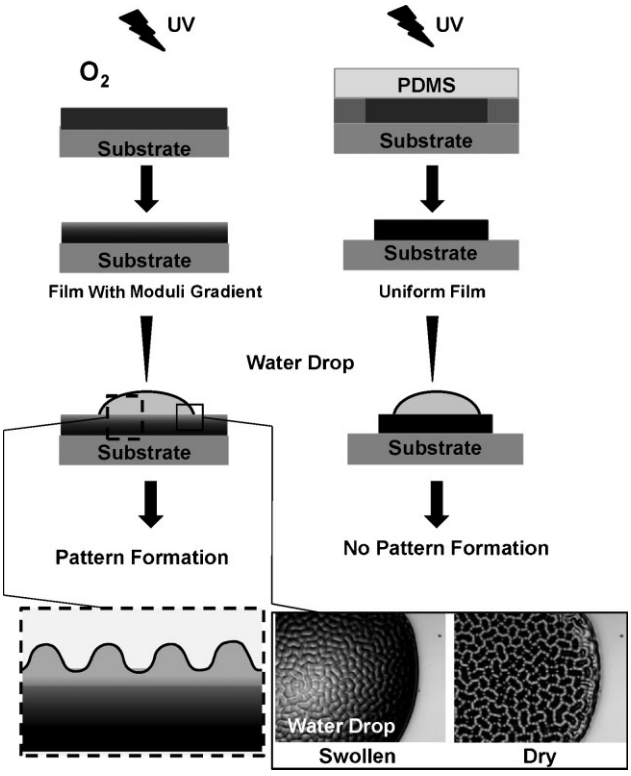

Figure 1. Schematic showing the fabrication of PHEMA films either with a modulus gradient or with a uniform modulus with depth. The spun-cast precursor solution is exposed to UV either open to air or covered with PDMS. Patterns are spontaneously formed for films with a modulus gradient when the film is exposed to water and are stable even when the film is dried.

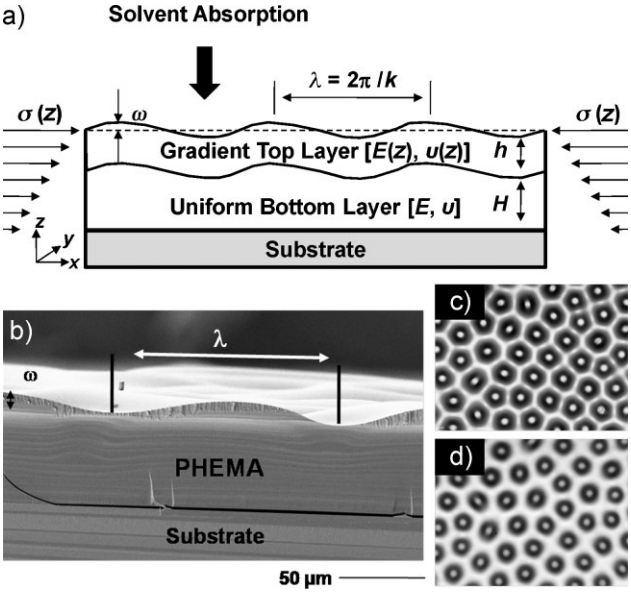

Figure 2. a) Model system composed of two layers: bottom layer with uniform mechanical properties and a thinner top layer with gradient mechanical properties due to oxygen inhibition during photocrosslinking. b) Cross-sectional SEM image of PHEMA film. c,d) Optical image of dry and swollen films, respectively.

intensity, and film thickness. Our approach specifically investigates the influence of EGDMA concentration and film thickness. We would like to point out that our system differs from the UV-cured coatings where a hard elastic skin is generally formed above a softer elastic or viscous layer.[24] We created a soft layer that gradually stiffened with depth (Fig. 1).

When a droplet of water was placed on the gradient PHEMA film surface, four distinctive wrinkling patterns, including random worms, lamellae, peanuts, and long-range ordered hexagonal patterns, were formed spontaneously and transited with an increase in EGDMA concentration (Fig. 3). The patterns were confined within the trace of the water droplet, and remained stable upon water evaporation (Fig. 2). The patterns were also observed in both the hydrated and dried states, with no change in the pattern morphology or stability, even after complete immersion in water for several days. We suspect that the gradient crosslinking density plays a critical role in the evolution of surface patterns and their ordering together with lateral confinement of the gel, promoting anisotropic osmotic pressure along the film thickness. Supporting this, we observed no pattern formation in samples containing the same amount of EGDMA and photoinitiator when they were covered with a flat PDMS slab during UV exposure (Fig. 1). Although PDMS is permeable to oxygen, we believe that the PDMS acts as a barrier that limits oxygen diffusion (especially compared to the open system) into the precursor solution, leading to a relatively uniformly cured gel and no pattern formation. We note that this observation is different from prior reports in uniformly cured and swollen poly(acrylamide) gel systems.[17,20] We attribute it to the higher modulus, and as a result less swelling, of PHEMA gels over poly(acrylamide) gels. In our PHEMA-gel systems with modulus gradients, the top surface swelled extensively in comparison to the underlying layers, leading to the formation of surface wrinkling patterns (Fig. 3). No patterns were observed when the EGDMA concentration was $\geq$4 wt%, indicating that the film was highly crosslinked to resist swelling by water, leading to an internal osmotic pressure below the wrinkling threshold.

By simply varying the crosslinker concentration and the initial film thickness, we generated a library of surface patterns with controlled ordering and size (see Fig. S2, Supporting Information). The pattern ordering was nearly independent of the film thickness, whereas the characteristic wavelength (λ) (40–120 μm) increased linearly with film thickness (30–250 μm; Fig. 4), and was dependent on the film modulus. This is consistent with the observation by Tanaka et al.[17] For films of equal thicknesses, λ increased with decreasing crosslinker concentration. We note that the order and characteristic wavelength of the patterns formed in swollen states and dry conditions are nearly identical (Figs. S2 and S3, Supporting Information), and remained stable during subsequent swelling. Thus, the generated patterns can be used in both conditions. This observation is different from the constrained hydrogels where patterns are transient in nature

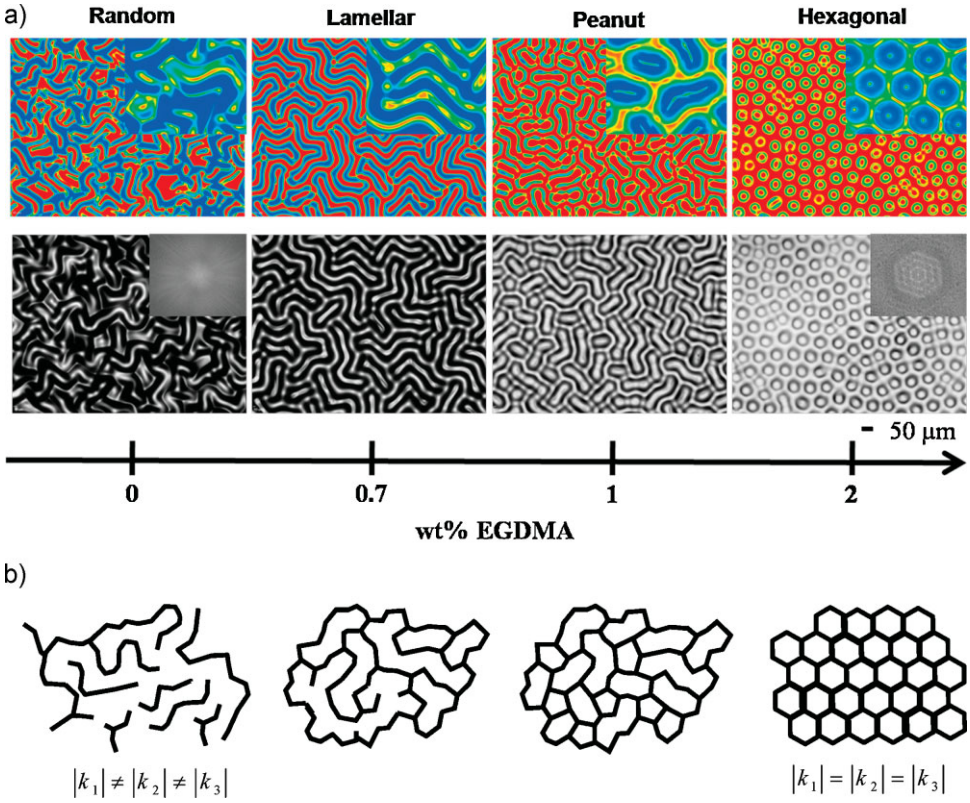

Figure 3. a) Optical images of patterns on the surfaces of DI-water-swollen PHEMA films. Top images are RGB colored with magnified insets and bottom ones are grayscale images. b) Schematic illustration of the wave pattern formation, where each wave consists of three wave vectors. When each wave vector has equal magnitude, a hexagonal pattern is obtained [17]. When the crosslinker concentration is decreased, more than one waves become unstable, distorting the hexagonal symmetry.

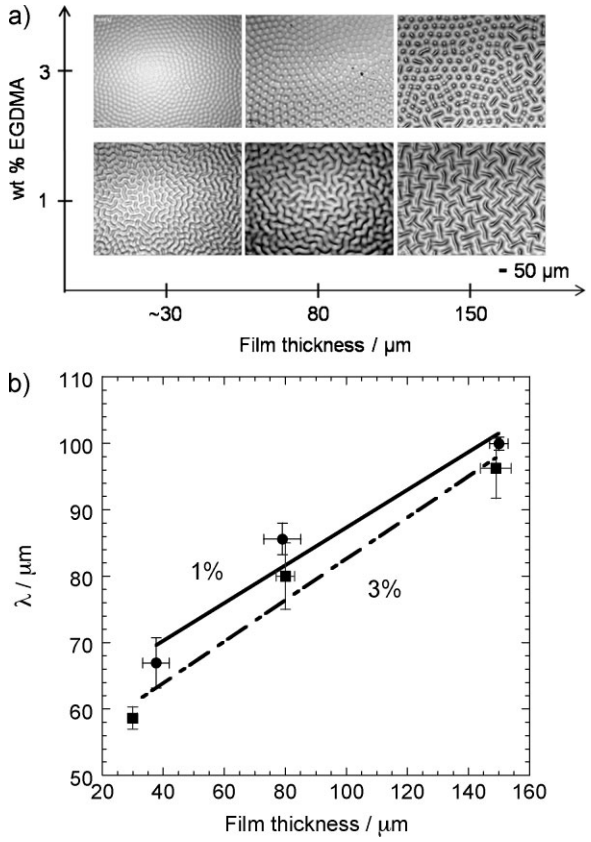

Figure 4. Optical images showing the change in pattern ordering with initial PHEMA film thickness. The characteristic wavelengths of the patterns increase linearly with film thickness and decrease in magnitude with increasing crosslinker concentration. The pattern ordering is dependent on the crosslinker concentration, but independent of film thickness.

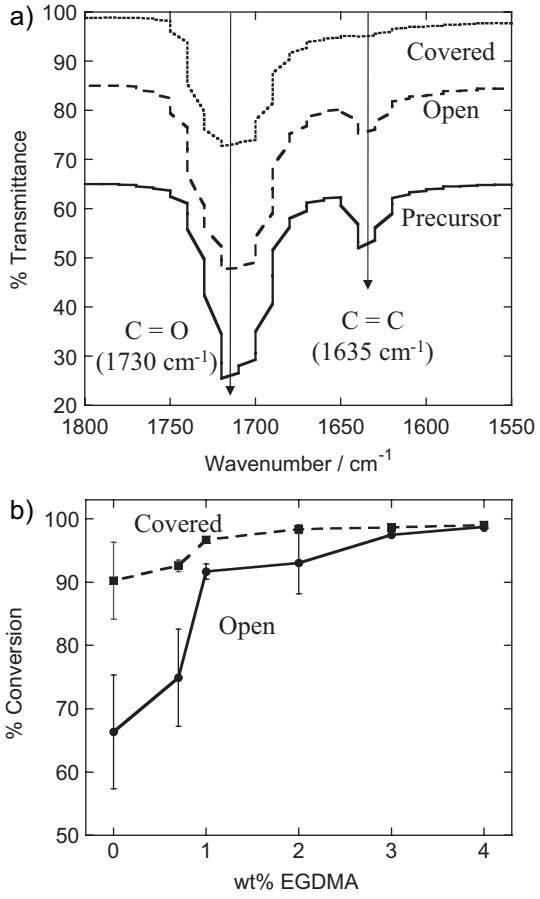

Figure 5. a) FTIR spectra for PHEMA without EGDMA: the precursor solution, polymerized film open to air, and polymerized film covered with PDMS. b) % Conversion of the vinyl bonds (C=C) in PHEMA films exposed to UV light while covered with PDMS in comparison to those open to air.

and disappear during drying.[17,20] We attribute this result to the transition of PHEMA from a rubbery (swollen) to glassy (dry) state during drying, which locks the equilibrium pattern, as the relaxation times are much larger than the time required for drying. PHEMA films were glassy in the pre-swollen dry state with a $T_g \approx 85$–$105\,^{\circ}C$ for 0–4 wt% EGDMA for uniform films and $T_g \approx 40$–$55\,^{\circ}C$ for gradient films (see Fig. S4, Supporting Information). For swollen films, the T_g dropped to less than 2 °C. Therefore, swollen films could easily buckle under in-plane compressive stress due to osmotic pressure, whereas the surface pattern became trapped upon drying. Consistent with our argument, when the PHEMA films were polymerized without EGDMA, followed by drying at 90 °C, the patterns were barely visible under the microscope.

To further investigate the nature of the formed gradients, we used attenuated total reflection Fourier transform infrared spectroscopy (ATR-FTIR) to assess the double bond (C=C) conversion at the surface of the crosslinked films. Crosslinked films (70 μm) attached to glass slides were placed on to the selenium crystal with the film surface facing the crystal and full contact between the crystal and film was maintained with a pressure clamp. The penetration depth of the beam for our system was calculated to be ~2 μm (see Experimental Section). The spectra for PHEMA films (Fig. 5a) indicates that the peak for the vinyl bond (~1635 cm^{-1}) from the precursor solution became smaller when the film was exposed to UV open to air (open), indicating the presence of unreacted double bonds, and almost disappeared when the precursor was covered with PDMS during UV exposure (covered). The conversion was calculated by comparing the vinyl peak areas before and after polymerization versus an internal standard, C=O (1730 cm^{-1}) peak (Fig 5b). Our results showed that for PHEMA without EGDMA, conversion was ~68% for an open system and ~90% for the covered system. For 0.7 wt% EGDMA, it was ~75% for an open system and ~93% for the covered system. For 2 wt% EGDMA, conversion was ~90% for an open system and ~98% for a covered system. These results indicate that UV exposure of precursor solutions open to air leads to a lower conversion at the surface, and higher conversions were obtained with increasing EGDMA concentration. The presence of unreacted groups after curing was also confirmed by DSC thermal analysis. When the crosslinked films were heated, a broad exothermic peak around 120–130 °C (corresponding to the thermal curing of the unreacted groups) was observed. This peak disappeared when the films were reheated after cooling (Fig. S4, Supporting Information) or swollen to equilibrium and dried at room temperature prior to measurements, indicating that the

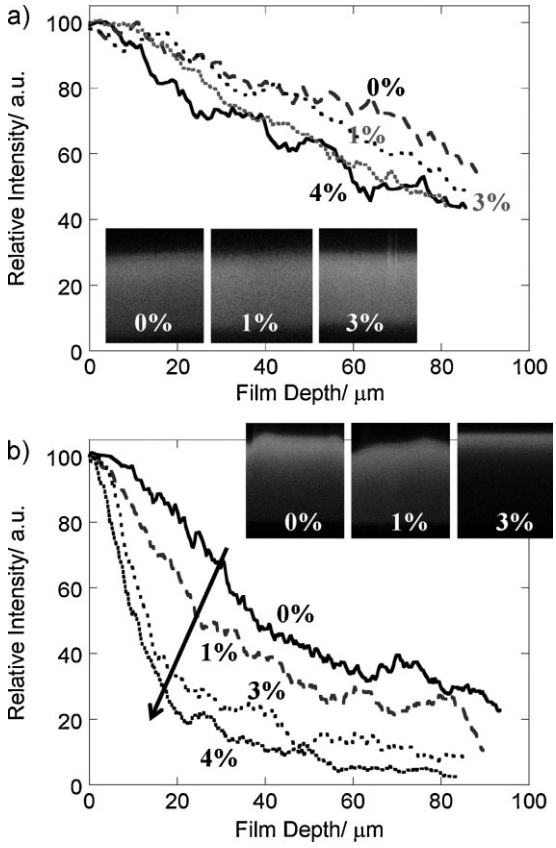

Figure 6. Confocal fluorescent microscopy depth profiles for photocrosslinked PHEMA films swollen to equilibrium in a FITC/H_2O solution. Films were fabricated by exposing the precursor solution to UV while the surface of the precursor was a) open to air or b) covered with PDMS. Inset pictures are confocal *xz*-scans of the swollen films, gray indicating the diffusion of FITC molecules within the gels at various EGDMA concentrations.

unreacted groups at the surface of the film leached out during swelling.

In order to characterize the depth profile of the modulus gradient, the films (~80-μm thick) were equilibrated in an aqueous fluorescein-5-isothiocyanate (FITC) solution (~3 mg mL^{-1}). The amount of diffused solvent in the hydrogel film is supposed to be related to the crosslinking density (either in gradient or uniform fashion, depending on the crosslinking system used). For uniform films (films covered with PDMS during crosslinking), the intensity (normalized to the highest fluorescence) of the FITC decreased gradually from 100 to 60 when assessed for depths up to 90 μm (Fig. 6a). This decrease is due to confinement of the gels, which leads to the water concentration in the gel gradually decreasing with depth. For gradient films (crosslinked in open air), the intensity profiles showed two distinctive regions (Fig. 6b) that started with a sharp decrease in FITC concentration up to 20–40-μm depth followed by a gradual decrease similar to the uniform films. The first region of the intensity-depth curve is attributed to the oxygen-diffusion gradient, and thus a crosslinking gradient, whereas the second part is attributed to the mechanical constraint by the rigid substrate. The steepness of the gradient increased with increasing crosslinker concentration, and the depth of crosslinking gradient (*h*) decreased with increasing crosslinker concentration. The values for *h* were ~39 μm for films without EGDMA, ~34 μm for 1 wt% EGDMA, ~27 μm for 3 wt% EGDMA, and ~ 22 μm for 4 wt% EGDMA. The reproducibility of the gradient was also confirmed by comparing the results for three samples per formulation and at least three different locations per sample. It should be noted that the maximum absolute fluorescent intensity was much higher at the surface for the gradient films than for the uniform films.

To better understand the effect of surface properties of the film on the final pattern formation, atomic force microscopy (AFM) was used to characterize the structural and mechanical properties of the crosslinked PHEMA films. Films (70-μm dry thickness) crosslinked open to air and covered by PDMS during curing, with a range of EGDMA concentrations were equilibrated in DI water prior to analysis. As seen in Figure 7a, PHEMA films with 0.7 wt% EGDMA and crosslinked in open air show: i) a sharp decrease in cantilever deflection (force) prior to the actual contact, ii) hysteresis between loading and retraction curves, and iii) a negative force required to retract the tip from the sample surface due to adhesion between the AFM tip and hydrogel film. Similar behavior was

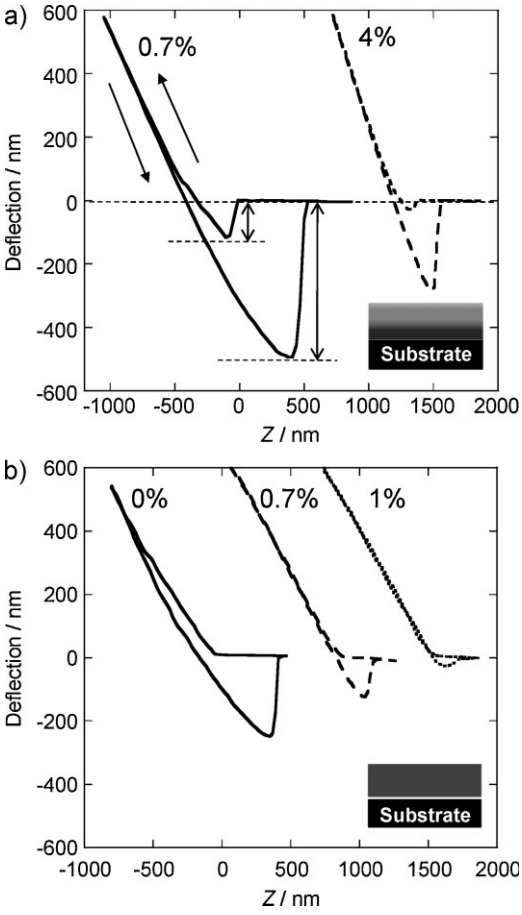

Figure 7. AFM force curves for swollen PHEMA films. Films were prepared by exposing the precursor solution to UV light: the top surface a) open to air creating a modulus gradient with thickness and b) covered with PDMS resulting in uniform modulus with thickness. Curves are shown for various EGDMA concentrations and are shifted along the horizontal axis for clarity.

observed when the PHEMA precursor solution was exposed to UV without EGDMA (see Fig. 7b). When the concentration of EGDMA was increased to 4 wt%, no patterns were observed, and the negative force prior to contact and the adhesive force were much lower in magnitude compared to the lower EGDMA concentrations that did form patterns. Further, the linear response in loading and unloading suggested the film was highly crosslinked. These features clearly indicate that at low EGDMA concentrations (<4 wt%) the gels were inhomogeneous with a weak boundary layer at the air–film interface.[25] Such negative force prior to contact was not present for any gels covered with PDMS, and the curves showed no hysteresis except for without EGDMA (Fig. 7b). Although a small adhesive force was observed for gels with EGDMA < 1 wt%, it completely disappeared at higher EGDMA concentrations. These results again support our hypothesis that a more uniform gel surface structure is obtained when the precursor solution is protected from oxygen diffusion during curing.

These results clearly confirm that curing films open to air generates crosslinking gradients with depth due to oxygen inhibition. The competition between oxygen diffusion through the air–film interface and oxygen consumption during curing leads to a film with a steeper crosslinking gradient at the surface and a more uniform gel near the substrate (Fig. 2b). Since the hydrogel films covered by PDMS were more uniform, AFM force curves were used to calculate the Young's modulus (E) of the uniform PHEMA films with varying crosslinker concentration according to a Hertz model for small indentations ($\delta < R/10$):[26,27]

$$F = k(z-\delta) = \frac{4}{3}\frac{E}{(1-\upsilon^2)}\delta^{3/2}R^{-1/2} \quad (2)$$

where the Poisson's ratio $\upsilon = 0.5$ for an incompressible gel (for uniform gels), the force constant of the cantilever $k = 0.06\ \mathrm{Nm}^{-1}$ (DNP, Veeco), and the radius of curvature of the tip $R = 500$ nm. By fitting the experimental force curve,[26] the Young's moduli of the PHEMA gels were in the range of ~200 kPa to ~3 MPa, depending on the EGDMA concentration (Table 1). The corresponding shear moduli obtained from shear rheology of the bulk gels are also included in Table 1 for comparison. A single E value for each composition obtained for uniform films is not valid for a gradient film; however, these values could be assigned as the upper modulus limit for the gradient films (i.e., area where oxygen inhibition is not significant, see Fig. 2b).

Table 1. Glass transition temperature (T_g), shear modulus (G), Young's modulus (E), and pattern ordering in PHEMA films as a function of crosslinker (EGDMA) concentration and equilibrium water fraction (ϕ_w).

EGDMA [wt%]	T_g [a] [°C]	ϕ_w	G [b] [kPa]	E [c] [kPa]	Pattern
0	~85	0.69 ± 0.01	31 ± 11	194 ± 44	Random
0.7	~87	0.58 ± 0.01	98 ± 1	283 ± 57	Lamella
1	~87	0.54 ± 0.06	133 ± 56	395 ± 89	Peanut
2	~85	0.52 ± 0.05	176 ± 28	1374 ± 342	Hexagonal
3	~92	0.45 ± 0.01	300 ± 23	1639 ± 215	Hexagonal
4	~104	0.41 ± 0.03	430 ± 40	2950 ± 557	No Pattern

[a] For dry films (swollen $T_g < 2^0$C for all samples except for 4 wt% EGDMA). [b] Shear rheology of bulk gels. Standard deviations are for 3 samples each. [c] Modulus values obtained from AFM force curves for uniform thin films (70 μm). Standard deviations are for 30 measurements each.

In a swollen gel, the instability is determined by the competing forces of osmotic pressure and lateral confinement. Tanaka et al. defined the osmotic pressure (P) for instability as follows[17]

$$P = \left(E_2^{1/2}\frac{kh}{3} - E_0^{1/2}\frac{1}{kh}\right)^2 + \frac{2}{3}(E_2E_0)^{1/2} \quad (3)$$

The critical pressure for buckling (P_c) with a critical wavelength (λ_c) is equal to

$$P_c = \frac{2}{3}(E_2E_0)^{1/2},\ k_c = \frac{2\pi}{\lambda_c} = \left(\frac{E_0}{E_2}\right)^{1/4}\frac{\sqrt{3}}{h} \quad (4)$$

which is roughly proportional to the average Young's modulus of a uniform gel ($P_c \approx E$) and independent of the film thickness (h), whereas the characteristic wavelength (λ_c) of the patterns is proportional to the film thickness and dependent on the modulus. For the gradient gels, the modulus of the film at the surface and deeper in the film differs much so that E_2 is approximated as the effective modulus for the surface (E^*) and E_0 is approximated as bulk modulus of the bottom region (E). The stability diagram is shown in Figure 8a for a wide range of E/E^*. Supporting our experimental results, the critical stress required to buckle films

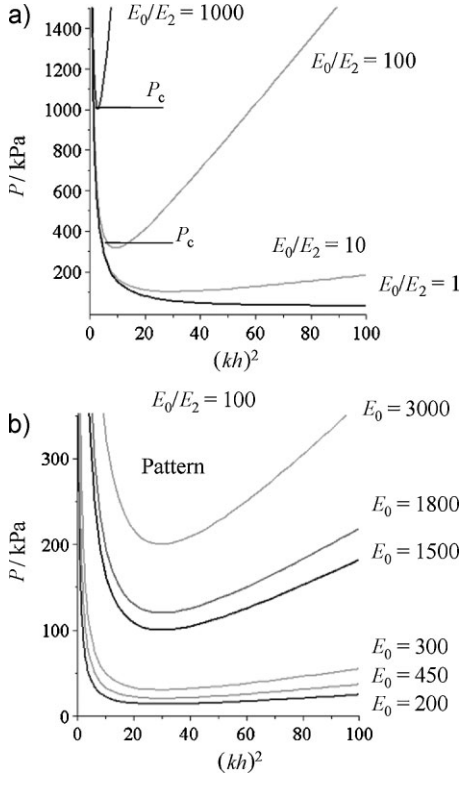

Figure 8. a) Pressure curves showing the effect of steepness. For pressures below the curve, the surface is flat, whereas the film buckles above the critical pressure (P_c). b) Pressure curves for pattern stability showing the effect of modulus for constant steepness.

increases significantly with increasing E/E^* values, which indicates a steeper gradient (high EGDMA concentration). In addition, for a constant E/E^* as the modulus increases, the pressure curve shifts to higher values (Fig. 8b). The order of the patterns is determined by the osmotic pressure, and can be explained using a similar approach to that of Benard's cell pattern.[28] A wave composed of three standing waves with wave vectors k_1, k_2, and k_3 construct a perfectly hexagonal pattern when $k_1 + k_2 + k_3 = 0$ and $|k_1| = |k_2| = |k_3|$ (Fig. S3, Supporting Information). This condition is satisfied for a swollen gel when $P = P_c$ with $k_c = |k_i|$ $(i = 1,2,3)$.[17,28] In practice, for a highly swollen gel, the osmotic pressure is always higher than the critical osmotic pressure, leading to more than one unstable mode growing simultaneously. Therefore, it has been difficult to obtain perfect hexagonal patterns.[17,19] Similarly, for bilayer systems, $k_3 = 0$. When the compressive stress is much greater than the critical stress, it leads to the formation of 1D ripples, $k_1 = k_c$ $(k_2 = 0)$, or 2D herringbone structures, $\sqrt{k_1 + k_2} = k_c$.[15]

In our case, the modulus gradient within the film makes it possible to control the critical osmotic pressure (Fig. 3), and thus the buckling modes. For EGDMA concentration $\geq$4 wt% ($E \geq 3$ MPa), the critical osmotic pressure is much higher than the osmotic pressure, thus no patterns form. At 2–3 wt% EGDMA loading, the modulus of the gels decreased to ~1.5 MPa and a highly ordered hexagonal pattern in the form of an array of convex lenses (honeycomb structure) was observed, suggesting that the osmotic pressure was close to the critical osmotic pressure. As the modulus of the gel continued to decrease (e.g., 1 wt% EGDMA) more than one mode became unstable, and the two individual hexagonal patterns coalesce into peanut-shaped features. At 0.7 wt% EGDMA loading, the features further coalesce to form lamellar patterns. When the film was formed without an external crosslinker, the modulus and hence the critical osmotic pressure was much lower than the osmotic pressure, resulting in completely random, worm-like patterns.

3. Conclusions

We have developed a simple and robust method to generate a wide range of osmotically driven surface patterns, including random, lamellar, peanut, and hexagonal structures, on hydrogels with moduli gradients. Hydrogels were fabricated by exposing a photocurable formulation of HEMA and EGDMA to UV light open to air and then swelling. The competition between the saturated oxygen consumption due to curing and oxygen diffusion into the film from the air–film interface (top surface) led to gradients of high to low crosslinking with depth. The steepness of the gradient increased and the depth of the gradient decreased with increasing EGDMA concentration. In particular, long-range ordered hexagonal patterns were observed when the osmotic pressure was close to the critical osmotic pressure. By tuning the modulus gradient, we were able to capture the order transition, where the initially formed hexagonal pattern collapsed into peanut shape, then lamellar and random worm patterns with the increase of osmotic pressure relative to the critical value. The modulus gradient, and hence osmotic pressure, was controlled by the EGDMA concentration, and the characteristic size of the patterns were determined by the initial film thickness. Patterns were stable in both swollen and dry states. Our method does not require the use of organic solvents for swelling, pre-patterning of the film surface, or coating of a second layer on the gel film surface. This versatile approach is potentially useful for diverse polymers to create complex patterns with a long-range order, which will impact a wide range of potential applications, including microlens arrays, tunable optical devices, sensors, and tissue engineering.

4. Experimental

Film Fabrication: Hydroxyethyl methacrylate (HEMA, 2 mL, 98%, from Alfa Aesar) monomers were mixed with Darocur 1173 (3 wt%, 60 μL, from Ciba Specialty) in a glass vial (20 mL) and exposed to UV light (UVP Black Ray, 8 mW cm^{-2}) for 60 s to obtain a viscous, partially polymerized PHEMA prepolymer solution. Additional Darocur 1173 (2 wt%, 40 μL) and ethylene glycol dimethacrylate (EGDMA) was added to the prepolymer to form a photocurable precursor solution. A series of precursor solutions either without or containing 0.7 wt% to 5 wt% EGDMA were prepared. They remained stable for several months when kept in dark. The precursor solution was spin-cast (Cee-100CB) onto a glass slide or silicon wafer, followed by exposure to UV light (Oriel Flood Exposure Source with 68951 Digital Exposure Controller, 500 W Hg Lamp) for 1 min to obtain a crosslinked PHEMA film. The thickness of the film was controlled by the spin speed (500–2 000 rpm) and time (10–30 s). In order to covalently attach the film to the substrate, glass slides were first functionalized with 3-(trimethoxysilyl)propyl methacrylate (TMS; 98%, Aldrich). The surface of the glass slides (1 × 1 inch coverslip) was covered with TMS (100 μL) immediately after UV–ozone treatment (Jelight UVO, Model 144AX) for 20 min, followed by two step annealing (100 °C for 30 min, then 110 °C for 10 min). Glass slides were then rinsed thoroughly in deionised (DI) water and dried overnight.

Wrinkling Patterns: The surfaces of the PHEMA films were covered with water to induce swelling assisted wrinkling. In a typical experiment, DI water (2 μL) was dropped onto the film surface with an automated dispenser (ramé-hart), and the covered region was allowed to swell for 20 min in order to fully develop the patterns. The water drop dried in ~25 min, which was long enough for the patterns to reach their equilibrium state.

Characterization: The dry thickness of the crosslinked film was measured by an optical profilometer (Alpha Step 200, Tencor). The patterns were characterized by optical microscopy (Olympus BX61) and scanning electron microscopy (SEM, FEI Strata DB235 Focused Ion Beam, 5 kV, film gold-coated). The surface mechanical properties of the gels were measured by atomic force microscopy (AFM). The AFM used was a Bioscope (DAFM-2X, Veeco) mounted on an epifluorescence microscope (Axiovert 100, Zeiss). For AFM studies, the films (~80 μm) were prepared on glass slides coated with TMS. Prior to the measurements, films were equilibrated in DI water for at least 15 min. Standard deviations were obtained from 30 consecutive measurements at different spots for each sample.

Reaction conversion of the crosslinked films at the film surface was characterized by ATR-FTIR performed using a Thermo Nicolet Nexus 470 FTIR with a Smart MIRacle ATR accessory (PIKE Technologies, Inc.) including single reflection ATR plate with zinc selenide (ZnSe) crystal, and a pressure clamp. Data were collected and analyzed using Omnic software. Spectra were collected using 64 scans at a resolution of 4 cm^{-1} between 630 and 4 000 cm^{-1}. Films (70 μm) crosslinked on glass slides were turned upside down (film surface facing the crystal), and full contact between the film and crystal surface was established using the pressure clamp. The depth of penetration was calculated as follows:

$$d_p = \frac{\lambda}{2\pi\left(n_c^2 \sin^2\theta - n_p^2\right)} \quad (5)$$

where λ is the wavelength of light, θ is the angle of incidence of IR beam (45°), n_c is the refractive index of ZeSe crystal (2.4) and n_p is the refractive index of the sample (~1.5 for PHEMA).

Differential scanning calorimetry (DSC) experiments were performed using a TA Instruments Q2000 DSC. Samples were heated to 170 °C and cooled to 1 °C, both at 5 °C min^{-1}. The data were analyzed using the Universal Analysis 2000 software provided by TA instruments. The glass transition temperature, T_g, was taken as the midpoint of the change in slope in heat capacity curve.

Acknowledgements

The research is funded in part by National Science Foundation MRSEC DMR05-20020, an NSF CAREER award DMR-0548070 (SY), and a Fellowship in Science and Engineering from the David and Lucile Packard Foundation (JAB). We acknowledge the Penn Regional Nanotechnology Facility at the University of Pennsylvania for SEM use. Supporting Information is available online from Wiley InterScience or from the author.

Received: April 10, 2009
Published online: August 19, 2009

[1] C. M. Stafford, C. Harrison, K. L. Beers, A. Karim, E. J. Amis, M. R. Vanlandingham, H. C. Kim, W. Volksen, R. D. Miller, E. E. Simonyi, *Nat. Mater.* **2004**, *3*, 545.
[2] E. Schaffer, T. Thurn-Albrecht, T. P. Russell, U. Steiner, *Nature* **2000**, *403*, 874.
[3] a) S. R. Quake, A. Scherer, *Science* **2000**, *290*, 1536. b) T. Thorsen, R. W. Roberts, F. H. Arnold, S. R. Quake, *Phys. Rev. Lett.* **2001**, *86*, 4163.
[4] a) A. Sidorenko, T. Krupenkin, A. Taylor, P. Fratzl, J. Aizenberg, *Science* **2007**, *315*, 487. b) D. P. Holmes, A. J. Crosby, *Adv. Mater.* **2007**, *19*, 3589.
[5] a) A. K. Geim, S. V. Dubonos, I. V. Grigorieva, K. S. Novoselov, A. A. Zhukov, S. Y. Shapoval, *Nat. Mater.* **2003**, *2*, 461. b) H. Lee, B. P. Lee, P. B. Messersmith, *Nature* **2007**, *448*, 338. c) E. P. Chan, E. J. Smith, R. C. Hayward, A. J. Crosby, *Adv. Mater.* **2008**, *20*, 711. d) P. C. Lin, S. Vajpayee, A. Jagota, C. Y. Hui, S. Yang, *Soft Matter* **2008**, *4*, 1830.
[6] S. Yang, G. Chen, M. Megens, C. K. Ullal, Y. J. Han, R. Rapaport, E. L. Thomas, J. Aizenberg, *Adv. Mater.* **2005**, *17*, 435.
[7] E. P. Chan, A. J. Crosby, *Adv. Mater.* **2006**, *18*, 3238.
[8] D. Chandra, S. Yang, P. C. Lin, *Appl. Phys. Lett.* **2007**, *91*, 251912.
[9] a) C. S. Chen, M. Mrksich, S. Huang, G. M. Whitesides, D. E. Ingber, *Science* **1997**, *276*, 1425. b) A. I. Teixeira, G. A. Abrams, P. J. Bertics, C. J. Murphy, P. F. Nealey, *J. Cell Sci.* **2003**, *116*, 1881.
[10] N. Bowden, S. Brittain, A. G. Evans, J. W. Hutchinson, G. M. Whitesides, *Nature* **1998**, *393*, 146.
[11] a) J. Groenewold, *Phys. A* **2001**, *298*, 32. b) S. J. Kwon, J. G. Park, *J. Phys. Chem. C* **2007**, *111*, 4404.
[12] C. M. Stafford, B. D. Vogt, C. Harrison, D. Julthongpiput, R. Huang, *Macromolecules* **2006**, *39*, 5095.
[13] a) E. P. Chan, A. J. Crosby, *Soft Matter* **2006**, *2*, 324. b) R. C. Hayward, B. F. Chmelka, E. J. Kramer, *Macromolecules* **2005**, *38*, 7768. c) K. Efimenko, M. Rackaitis, E. Manias, A. Vaziri, L. Mahadevan, J. Genzer, *Nat. Mater.* **2005**, *4*, 293.
[14] a) R. Huang, *J. Mech. Phys. Solids* **2005**, *53*, 63. b) P. C. Lin, S. Yang, *Appl. Phys. Lett.* **2007**, *90*, 3.
[15] X. Chen, J. W. Hutchinson, *J. Appl. Mech. -Trans. ASME* **2004**, *71*, 597.
[16] a) D. Breid, A. J. Crosby, *Soft Matter* **2008**, *5*, 425. b) J. Y. Chung, A. J. Nolte, C. M. Stafford, *Adv. Mater.* **2009**, *21*, 1358.
[17] T. Tanaka, S. T. Sun, Y. Hirokawa, S. Katayama, J. Kucera, Y. Hirose, T. Amiya, *Nature* **1987**, *325*, 796.
[18] a) J. S. Sharp, R. A. L. Jones, *Phys. Rev. E* **2002**, *66*, 011801. b) E. Sultan, A. Boudaoud, *J. Appl. Mech. -Trans. ASME* **2008**, *75*, 051002. c) A. Baffoun, H. Haidara, D. Dupuis, P. Viallier, *Langmuir* **2007**, *23*, 9447.
[19] H. Tanaka, H. Tomita, A. Takasu, T. Hayashi, T. Nishi, *Phys. Rev. Lett.* **1992**, *68*, 2794.
[20] V. Trujillo, J. Kim, R. C. Hayward, *Soft Matter* **2008**, *4*, 564.
[21] a) T. Hwa, M. Kardar, *Phys. Rev. Lett.* **1988**, *61*, 106. b) S. J. Kwon, J. G. Park, S. H. Lee, *J. Chem. Phys.* **2005**, *122*, 031101. c) A. Onuki, *J. Phys. Soc. Jpn.* **1988**, *57*, 703. d) K. Sekimoto, K. Kawasaki, *J. Phys. Soc. Jpn.* **1987**, *56*, 2997. e) T. Tanaka, D. J. Fillmore, *J. Chem. Phys.* **1979**, *70*, 1214. f) D. S. Zhang, M. O. de la Cruz, *Macromolecules* **2008**, *41*, 6612.
[22] a) C. Decker, A. D. Jenkins, *Macromolecules* **1985**, *18*, 1241. b) A. K. O'Brien, C. N. Bowman, *Macromol. Theory Simul.* **2006**, *15*, 176.
[23] A. K. O'Brien, C. N. Bowman, *Macromolecules* **2006**, *39*, 2501.
[24] M. H. Godinho, A. C. Trindade, J. L. Figueirinhas, L. V. Melo, P. Brogueira, A. M. Deus, P. I. C. Teixeira, *Eur. Phys. J. E* **2006**, *21*, 319.
[25] a) V. I. Uricanu, M. H. G. Duits, R. M. F. Nelissen, M. L. Bennink, J. Mellema, *Langmuir* **2003**, *19*, 8182. b) D. C. Lin, E. K. Dimitriadis, F. Horkay, *J. Biomech. Eng. -Trans. ASME* **2007**, *129*, 430. c) D. C. Lin, E. K. Dmitriadis, F. Horkay, *J. Biomech. Eng. -Trans. ASME* **2007**, *129*, 904.
[26] J. Domke, M. Radmacher, *Langmuir* **1998**, *14*, 3320.
[27] M. Radmacher, in *Methods in Cell Mechanics Vol. 83*, (Eds.: B. Jena, H. Hörber), Elsevier Academic Press, San Diego, CA **2007**, p. 347.
[28] T. Tanaka, *Physica A* **1986**, *140*, 261.